HYDROTHERMAL SYNTHESIS OF SHAPE SELECTIVE SnS NANOSTRUCTURES: GROWTH AND OPTICAL PROPERTIES

B Mondal[1*]

Abstract

SnS nanostructures of various morphologies are synthesized by a Polyacrylamide (PAM) assisted hydrothermal process. The morphology of the nanostructures changes with hydrothermal temperature (T_H) keeping the hydrothermal time constant at 2 hours. The synthesized nanostructures are characterized by XRD, FTIR, TGA, UV-Vis., FESEM and HRTEM. The remarkable observation is that SnS prefers sheet like structures during their growth. However, morphology changes from nanoparticles, agglomerated nanosheets to micron size bars or spindles with varying T_H. TEM images show the nanosheets are single crystalline. The Photoluminescence (PL) shows a broad emission peak at 468nm due to indirect band transition. The intensity of the PL spectra increases with increase in T_H.

[1*]Department of Physicss, Bankim Sardar College Tangrakhali, Canning, 24 Parganas (South) 743329, India. Tel: 91-9874620532, E-mail:*biswajitmondal.phy@gmail.com*

***CorrespondingAuthor:** B Mondal
*Department of Physicss, Bankim Sardar College Tangrakhali, Canning, 24 Parganas (South) 743329, India. Tel: 91-9874620532, E-mail:*biswajitmondal.phy@gmail.com*

DOI: 10.53555/ecb/2020.9.8.02

Introduction

Sulfide nanostructures are attracting much attention to both theoretical and experimental researchers for their fascinating properties and potential applications. Tin sulfide being an IV-VI semiconductor has several binary compounds such as SnS, Sn_3S_4, Sn_2S_3 and SnS_2. The orthorhombic herzenbergite structure of tin sulfide (SnS) is structural analogue to black phosphorous i.e. the 'Sn' and 'S' atoms are tightly bonded in a layer and the layers are bonded by weak van der Waals forces (**1**). SnS is usually a p type semiconductor with a band gap of 1.2eV, a value close to that of silicon, and acceptor levels are created by double ionized 'Sn' vacancies (**2**). The optical properties of SnS vary depending on the synthetic or fabrication method (**3**), but most work agrees on a direct band gap at 1.296eV and an indirect band gap at 1.095eV (**4**). It has some advantages relative to other sulfide materials such as elements being abundant in nature, stable under ambient conditions and not posing any health and environmental hazards. The narrow band gap and unique structural property of SnS makes it potential candidate for applications as solar absorber in thin film solar cell (**5**) and near infra-red detector **(6**), holographic registrar system (**7**), photoconductors (**8**), as photovoltaic materials (**9,10**) with high conversion efficiency (~25%) (**11**). There are many traditional methods such as template assisted electrodeposition (**12**), soft chemical (**13**), solvothermal/hydrothermal (**14**), Solid–vapor interaction (**15**), direct vapor transport method (**16**), stoichiometric composition technique (**17**), physical vapor transport method (**18**) and Bridgman– Stockbarger technique (**19**), SILAR technique (**20**), for synthesis of SnS nanoparticles (**21**), nanobelts, nanosheets, nanorods, nanoflowers etc. But, one pot hydrothermal synthesis of single crystalline SnS nanoshets still remained a grand challenge by low temperature, cost effective way without taking help of any complicated instrument and following any strenuous chemical extraction process. In this paper, we report a very simple, low temperature hydrothermal process to synthesize SnS nanoparticles, agglomerated nanosheets to micron sized nanobars or spindles. However, this template less solution-based synthesis is characterized by few deficiencies such as relatively low yields, irregular and mixed morphologies.

Experimental

All the chemicals were used as received i.e. without further purification. 1.0gm of polyacrylamide (MW>5,000,000, Poole, England) is mixed with 200mL of distilled water and stirred for nearly 15 min., kept for one week to get matured and used as stock solution. 0.3gm of thiourea (CH_4N_2S, Merck, Mumbai, India) and 5mL of PAM are gradually added to 0.5gm of tin chloride ($SnCl_2$, $2H_2O$, Merck, Mumbai, India) solution while stirring. The mixture is transferred to a teflon lined stainless steel autoclave and heated at different temperatures in a hot air oven after filing nearly 80% of its total volume by distilled water. The autoclave is heated at different hydrothermal temperatures (T_H) for two hours (2 h). The gray precipitate obtained from the autoclave after cooling it to room temperature naturally, is collected by centrifugation and dried at 80^0C for 1 h in a hot air oven and used for further characterization.

Instrumental

The optical, morphological, microstructural and physical properties of the final product were investigated. The phase purity and crystal structure of the samples were characterized by powder X-Ray Diffraction (XRD) by a Rigaku (Washington, USA), diffractmeter. Interaction between 'Sn', 'S' and PAM was studied by Fourier Transform Infrared (FT-IR) spectroscopy (FT-IR-8400S, Simadzu, USA). Thermal stability of SnS is investigated by Thermogravimetric Analysis (TA Inst., Qsdt 600, USA). A little amount of the SnS samples is ultrasonically dispersed in water to measure Ultra Violet-Visible (UV-Vis.) absorption spectra and Photoluminescence (PL) emission spectra by using Cary 5000 (Varian, USA) and Fluoromax 4 (Horiba Jobin Yvon, Kyoto, Japan) with excitation at 250nm, respectively. The morphology, size and crystal structure of the SnS samples were determined by Transmission Electron Microscopy (TEM, JEM 2010) having an Energy Dispersive X-ray Analysis (EDAX) apparatus at 200kV for composition analysis and Field Emission Scanning Electron Microscopy (FESEM, JSM 6700F, Tokyo, Japan).

Results and Discussion

XRD Studies

The XRD pattern reveals overall crystal structure and phase purity of the synthesized SnS nanostructures. The XRD pattern of SnS samples heated at different T_H (120^0C, 160^0C, 200^0C & 240^0C) is given in **Figure 1 (a to d** respectively**)**. The diffraction peaks for the sample heated at 120^0C, consists of a few broad peaks of SnS nanoparticles and amorphous PAM. However,

crystallinity of the samples increase at elevated T_H and the peaks become gradually sharp. The diffraction peaks are indexed and matched to standard XRD pattern to an orthorhombic herzenberzite structure with space group of Pbnm, which agrees well with the reported values (a = 4.328 A^0, b = 11.19A^0 and c=3.978 A^0) from JCPDS card No. 14-0620. No characteristic peaks from impurities, such as elemental 'Sn' or other phase of tin sulfides or hydroxides are detected. Scherer formula (**22**) for the nanocrystals is expressed as, $d = \frac{0.9\lambda}{\Delta\theta \cos\theta}$

Where,'d' is the diameter of the nanocrystals to be determined, 'Δθ' is the full width at half maximum (FWHM) of XRD peaks expressed in radians and 'λ' is the wavelength of the X-ray used. Putting the values of above parameters in the Scherer formula from the XRD data; the size of the nanocrystals estimated at 40nm which is corroborated well with the size as represented in TEM images (**Figure 6a & b**). So, it is concluded that the as synthesized samples are SnS with different degree of crystellinity depending on the T_H.

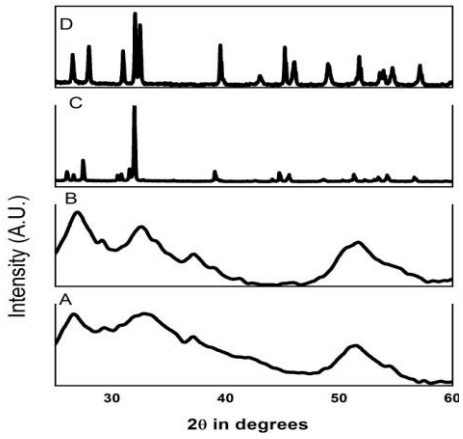

Figure 1: (a), (b), (c) & (d) shows XRD pattern of the samples heated at various T_H (120 ^{0}C, 160 ^{0}C, 200 ^{0}C & 240 ^{0}C respectively). The XRD pattern shows gradual increase in crystallinity at elevated T_H

FT-IR Studies

To confirm the presence of surfactant (PAM) on surfaces of the as synthesized nanocrystals and to investigate interaction of PAM with 'Sn'; FTIR spectra is recorded in the range of 400 to 4000cm^{-1} as shown in **Figure 2** for only PAM and SnS sample heated at 240^{0}C. Usual peaks for C–N stretching (around 1400cm^{-1}), –NH_2 bending (1655–1620cm^{-1}), C=O stretching (1660cm^{-1}), –CH_2 stretching (3083$cm^{-1}$and 2980cm^{-1}) and –NH_2 stretching (3450cm^{-1}) are reported (**23**) in the pristine PAM spectrum. Significant changes in the spectra of SnS nanocrystals; at 1660cm^{-1} due to C=O stretching and in the range 500-800cm^{-1} due to Sn-O-Sn stretching mode are observed. This indicates that the surfactant is present on the SnS nanocrystals. The broad band between 3200 and 3600cm^{-1} and the band centered at1622cm^{-1} in the spectra was assigned to -O-H stretching and deformation vibrations of weak bound water molecules in the materials (**24**). In nutshell, two significant changes are observed between the FTIR spectra of PAM and SnS nanocrystals (T_H≈ 240^{0}C). For SnS nanocrystals, C=O stretching (1660cm^{-1}) is red-shifted compared to PAM and both peaks corresponding to Sn–O–Sn stretching (655cm^{-1} and 494cm^{-1}) is also red-shifted. These red shifts of FTIR peaks indicate strong interaction between 'Sn' and 'O' of carbonyl (C=O) group. In short, PAM is attached to SnS through carbonyl group of PAM.

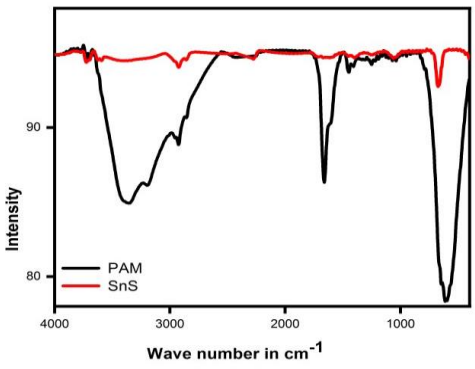

Figure 2: FT-IR spectra of pure PAM and SnS nanostructures displays two significant changes relative to the pristine PAM

TGA analysis

TGA analysis is undergone with a view that it will reveal exact decomposition and crystallization temperature of SnS and it will enable us to predict the thermal stability and purity of SnS from the decomposition temperature. The TGA curves of samples heated at different T_H; have three regions where mass losses have been occurred. First one from 60^0C to 170^0C (~ 11%) is due to adsorbed water on the surface and other volatile impurities **(25)**, second one between 230^0C to 315^0C (~ 17%) due to decomposition of residual amide groups and the third nearly 13% mass loss at 455^0C is attributed to complete decomposition of SnS nanocrystals. It may be noted from **Figure 3** that the decomposition temperature of SnS diminished due to the nanometric dimension. As T_H increases the amount of mass loss at each region decreases and at maximum T_H (~240^0C) only the third region is predominant (~48%). The samples do not show the characteristic melting peak of 'Sn' at 230^0C which indicates that metal 'Sn' is completely converted into SnS.

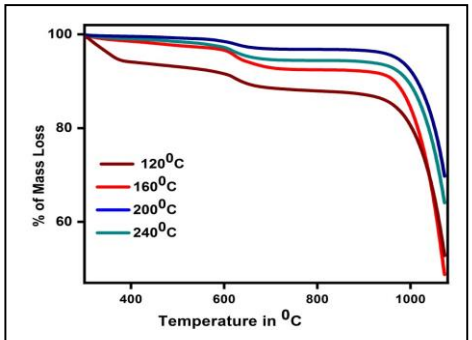

Figure 3: TGA of four samples shows the mass loss and the thermal stability of SnS nanostructures

UV-Vis. spectra

UV-Vis. absorption spectra were recorded with a hope that it will help to explore the band gap, crystellinity, and composition of the semiconducting nanocrystal. The absorption spectra of the samples obtained from hydrothermal method have broadness from 800nm to 200nm as shown in **Figure 4a** with an absorption onset at 400nm indicating they are better absorber materials than the commonly used CdSe NPs. Moreover, band gap is calculated by using Tauc's equation (**26**), $\alpha h\nu^n = K(h\nu - Eg)$

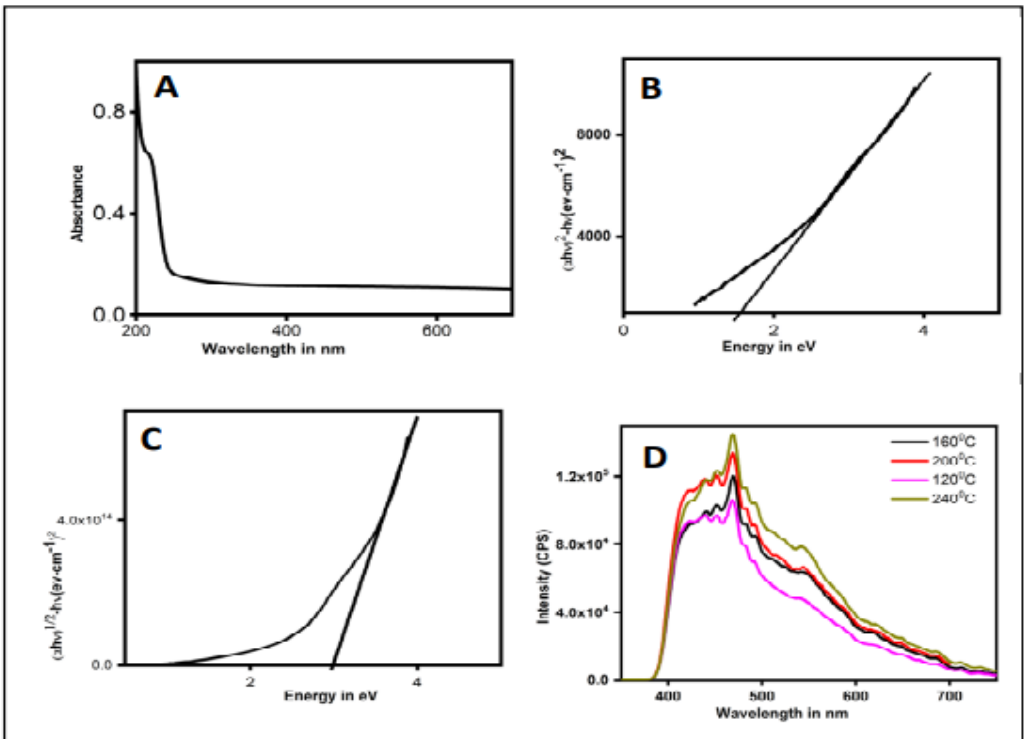

Figure 4: (a). UV-Vis. absorption spectra of the SnS nanostructures cover whole visible region (b). Direct band gap of SnS nanostructure is estimated by using Tauc's formula which comes out at 1.6eV (c). Indirect band gap of the sample is calculated at 2.8eV (d). PL spectra of four SnS samples with a peak at around 468nm and the intensity of the PL spectra increases with increasing T_H

Where, 'K'is a constant and 'n'is a number that characterizes the nature of transition involved. It is well known that the 'n' value is 2 and 2/3 for direct allowed and forbidden transitions, respectively, while the value is 1/2 and 1/3 for indirect allowed and forbidden transitions, respectively. To calculate the direct and indirect band gap; the functions $(\alpha h\nu)^2$ - hν and $(\alpha h\nu)^{1/2}$-hν are plotted against energy (hν). Then, a tangent is drawn at the point of inflection and extrapolated to cut x-axis. The value of the 'x' obtained in terms of the energy is the band gap energy. The calculated direct and indirect band gap energy is 1.6eV and 2.8eV respectively (**Figure 4b**&**4c**). Relatively high band gap energies of the samples obtained by hydrothermal method is due to formation of very small size SnS nanocrystals leading to increase in band gap energy because of quantum confinement. The increase in band gap energy (~ 0.204eV) of direct band gap semiconducting nanocrystals is given by modified Brus equation (**27**),

$$\Delta E_b = E_b^{eff} - E_b^{bulk} = \frac{h^2}{8\mu R^2} - \frac{1.8e^2}{R\varepsilon}$$

$$\frac{1}{\mu} = \frac{1}{m_e^*} + \frac{1}{m_h^*}$$

Where, 'h' is plank's constant, 'e' is the charge of electrons, 'R' is the radius of nanocrystals, 'μ' is the reduced mass and 'ε' is static dielectric constant and is equal to 14. As agglomerated very small size nanocrystals are obtained at lower T_H; quantum confinement will be obvious. At relatively higher T_H; though micron size nanocrystals are observed in FE-SEM and TEM images they are consisted of nanosize sheets. So, phenomena of quantum confinement can take place for them also.

P L Spectra

PL spectra are a very efficient, non-destructive, contactless technique used to characterize and evaluate quality of surfaces and interfaces as well as to probe defect levels within the material. The room temperature PL spectra of the SnS samples dispersed in water show two peaks one broad peak at 437nm (UV emission) and other at 468nm (blue emission) contrary to the emission peaks of the other phases of tin sulfide (**Figure 4d**). However, absence of direct band to band emission at 950nm of SnS lies outside the spectra due to the instrumental incapability. Indirect band gap of the samples being 2.8eV, the emission at 468nm is ascribed to indirect band to band transition and the emission at 437nm may be assigned to various defects. The broad emission spectra of the SnS samples may arise from various defects such as high density of sulfur and tin vacancies introduced during the synthesis process. Besides sulfur and tin vacancies, various kinds of defects such as interstitials, stacking fault have also been introduced in the nanocrystals. Such broadening of emission spectra due to various defects has also been reported earlier (**28, 29**). However, gradual increase in intensity with T_H, indicates the crystallinity of the samples improves at elevated T_H.

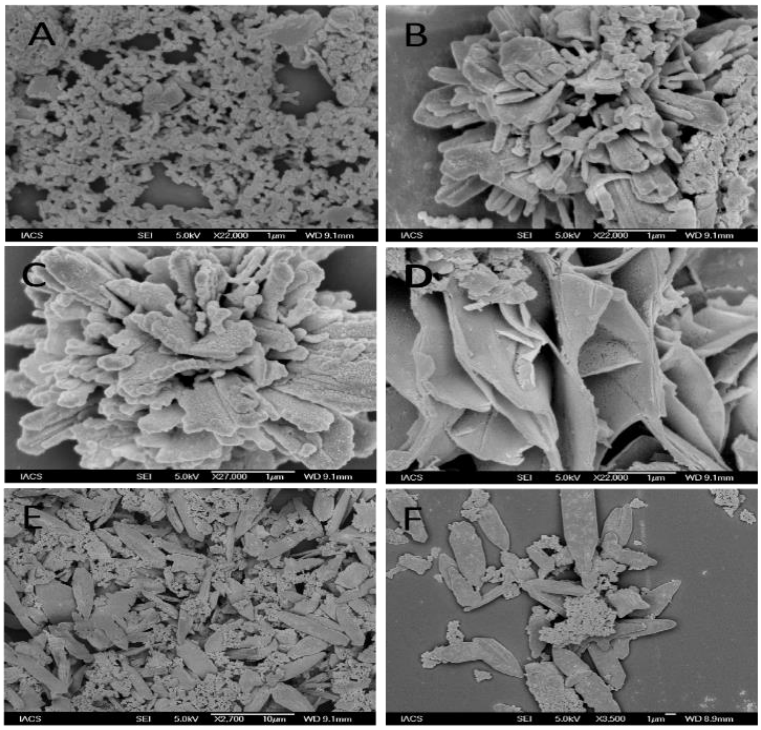

Figure 5: (a) FE-SEM image shows only agglomerated SnS nanoparticles at 120^{0}C for 2h (b) SnS sample heated at 160^{0}C shows agglomerated 2D sheets with some nanoparticles still present (c) SnS sample heated at 200^{0}C show only agglomerated SnS 2D sheets (d) Magnified image of SnS sheets shows their thickness is in the nanometric dimension (e) When the sheets are heated at 240^{0}C they agglomerate and form micron size nanobars & (f) Magnified image of nanobars show they their thickness is also in micron order

Growth Mechanism of SnS Nanostructures

In hydrothermal solution, Sn ions are attached to PAM chains through carbonyl group and form a complex ion in the solution.

$$Sn^{2+} + \left(CH_2CHCONH_2\right)_n \longrightarrow \left[Sn\left(CH_2CHCONH_2\right)_n^{2+}\right]$$

Meanwhile, thiourea releases H_2S gas.

$$CS\left(NH_2\right)_2 \longrightarrow NH_2CN + H_2S$$

$$H_2S \longrightarrow S^{2-} + 2H^+$$

H_2S gas reduces Sn ions to form SnS which act as nucleation cites on the PAM chains.

$$\left[Sn\left(CH_2CHCONH_2\right)_n^{2+}\right] + S^{2-} \longrightarrow \left[SnS\left(CH_2CHCONH_2\right)_n\right]$$

For layered crystal semiconductors, 0D or 3D nanocrystals are a metastable state, which has the tendency to transform to more stable 2-dimensional (2D) nanosheets. The size of the nanosheets varies from 40nm to 100nm, and they are rectangular in shape as shown in FE-SEM and TEM images. When the mixture is heated at relatively low T_H SnS NPs are formed with PAM adsorbed on the surfaces (**Figure 5a**). With passage of time, the NPs agglomerate to form SnS nanostructures (**Figure 5b**). As most layered crystal structures prefer to grow in 2D structures, at the initial stage 2D SnS nanostructures are formed. When T_H increased, SnS flower like structure are formed due to electrostatic attraction agglomerating the 2D sheets (**Figure c & d**). Here, at relatively higher T_H; generated high pressure can also lead to form the flower like structures. Again if the T_H is further increased keeping the hydrothermal time constant; the nanostructures are fused together to form micron size bars or spindles due to high temperate and high generated pressure inside the autoclave (**Figure 5e & f**).

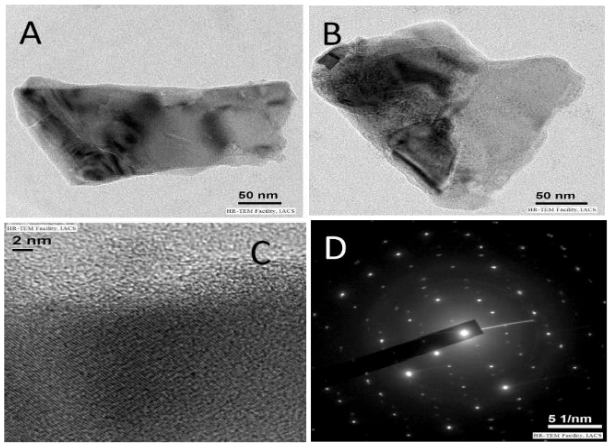

Figure 6: (a) HR-TEM image shows a SnS nanosheet. The thickness of the sheet is 30-40nm which is evident in the image (b) Image of relatively bigger SnS nanosheet (c) HR-TEM image of SnS which shows good crysttalinity of the sample & (d) SAED pattern of the synthesized SnS nanostructures

Transmission Electron Microscopy (TEM) reveals the microstructural and crystallographic orientation of the nanocrystals. Figure **6a**&**b** displays SnS nanosheets which are separated from flower like structures during ultrasonication for preparation of TEM sample. **Figure 6c** demonstrates crystallinity of SnS nanostructures. **Figure 6d** and **Figure 7** shows SAED and EDAX of SnS respectively and figures confirm that the nanostrucutres are composed of SnS nanocrystals with good crysttalinity.

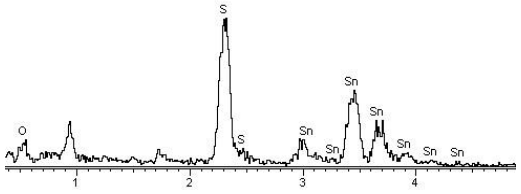

Figure 7: EDAX spectrum confirming that the nanostructures are composed of Sn & S

Conclusion

SnS nanosheets and micron sized nanorods or spindles were synthesized in a simple, low temperature hydrothermal process using PAM as surfactant as well as versatile soft template which helps SnS to grow along the PAM chain. A plausible growth mechanism for the nanorods is developed where PAM acts as surfactant as well as soft template to direct the growth process along the PAM chain.

Acknowledgement

BM acknowledges DST Unit on Nanoscience and Centre for Nanotechnology at Indian Association for the Cultivation of Science for infrastructural facilities. The author thanks Council of Scientific and Industrial Research (CSIR; New Delhi; India) for the fellowship. Author also acknowledges Prof. Shyamal Kumar Saha for useful discussions.

References:

1. Surfactant-Assisted Synthesis of SnS Nanowires Grown on Tin Foils; Subhendu K. Panda, Anuja Datta, Apurba Dev, Soma Gorai, and Subhadra Chaudhuri, Crystal Growth & Design, Vol. 6, No. 9, 2006.
2. Facile synthesis of IV–VI SnSnanocrystals with shape and size control: Nanoparticles, nanoflowers and amorphous nanosheets; G. H. Yue, L. S. Wang, X. Wang , Y. Z. Chen, D. L. Peng; Nanoscale Res Lett (2009) 4:359–363.
3. Optical and photoelectric properties of SnS thin films prepared by chemical bath Deposition; A Tanusevski, Semicond. Sci. Technol. 18 (2003) 501–505.
4. Tetrahedral Zinc Blende Tin Sulfide Nano and Microcrystals; Eric C. Greyson, Jeremy E. Barton, and Teri W. Odom, small 2006, 2, No. 3, 368 – 371.
5. Facile synthesis of monodisperse, size-tunable SnS nanoparticles potentially for solar cell energy conversion; Hongtao Liu1, Yan Liu, Zan Wang and Ping He, Nanotechnology 21 (2010) 105707 (5pp).
6. The effect of anneal temperature on physical properties of SnS films;G.H. Yue, W. Wang, L.S.Wang, X. Wang, P.X. Yan, Y. Chen, D.L. Peng, Journal of Alloys and Compounds 474 (2009) 445–449.
7. Optimization of photoconductivity in vacuum-evaporated tin sulfide thin films M. Radot, Rev. Phys. Appl. (Paris) **18**, 345 (1977).
8. Optimization of photoconductivity in vacuum-evaporated tin sulfide thin films; J B Johnson, H Jones, B S Latham, J D Parker, R D Engelken and C Barber, Semicond. Sci. Technol. 14 (1999) 501–507.
9. Photovoltaic structures using chemically deposited tin sulfide thin films; David Avellaneda, M.T.S. Nair, P.K. Nair, Thin Solid Films 517 (2009) 2500–2502.
10. Photovoltaic Behavior of NanocrystallineSnS/TiO_2;Yu Wang, Hao Gong, Benhu Fan, and Guangxia Hu, J. Phys. Chem. *C* 2010, *114*, 3256–3259
11. Characterization and Optical Properties of the Single Crystalline SnS Nanowire Arrays; Vilas G. Pol, Swati V. Pol, and Aharon Gedanken, Langmuir 2008, 24, 5135-5139.
12. Size and Shape Control of Colloidally Synthesized IV-VI Nanoparticulate Tin(II) Sulfide; G. H. Yue, L. S. Wang , X. Wang , Y. Z. Chen, D. L. Peng, Nanoscale Res Lett (2009) 4:359–363.

13. Size and Shape Control of Colloidally Synthesized IV-VI Nanoparticulate Tin(II) Sulfide; Stephen G. Hickey, Christian Waurisch, Bernd Rellinghaus, and Alexander Eychmuller, JACS. 2008, *130*, 14978–14980.
14. Thioglycolic acid (TGA) assisted hydrothermal synthesis of SnSnanorods and nanosheets; Subhajit Biswas, Soumitra Kar, Subhadra Chaudhuri, Applied Surface Science 253 (2007) 9259–9266.
15. Spray pyrolytic deposition and characterization of SnS and SnS_2 thin films; B Thangaraju and P Kaliannan, J. Phys. D: Appl. Phys. 33 (2000) 1054–1059.
16. Optimization of photoconductivity in vacuum-evaporated tin sulfide thin films; J B Johnson, H Jones, B S Latham, J D Parker, R D Engelken and C arber, Semicond. Sci. Technol. 14 (1999) 501–507.
17. Crystal Growth and Characterisation of SnS_2**;** E.P. Trifonova and I.Y. Yanehev, V.B. Stoyanova, S. Mandalidis, K. Kambas and A.N. Anagnostopoulos, Materials Research Bulletin, Vol. 31, No. 8, pp. 919-924.1996.
18. Absorption edge of tin disulfide single crystals;Joy George, C. K. Valsala Kumari, and K. S. Joseph, J. Appl. Phys. 54 (9). September 1983.
19. The effect of pressure on the optical properties of 2H and 4H SnS_2;M J Powell, J. Phys. C: Solid State Phys., Vol. 10. 1977.
20. Growth and characterization of tin disulfide (SnS_2) thin film deposited by successive ionic layer adsorption and reaction (SILAR) technique; N.G. Deshpande, A.A. Sagade, Y.G. Gudagea, C.D. Lokhande, Ramphal Sharma, Journal of Alloys and Compounds 436 (2007) 421–426.
21. Synthesis of SnS Quantum Dots;YingXu, Najeh Al-Salim, Chris W. Bumby, and Richard D. Tilley, JACS. 2009, *131*, 15990–15991.
22. Preparation of gamma alumina thin membrane by sol-el processing and its characterization by gas permeation; Okubo, T.; Watanabe, M.; Kusakabe, K.; Morooka, S. Journal of Materials Science.**1990***25* 4822-4827.
22. Sonochemical Synthesis of SnO_2 Nanoparticles and Their Preliminary Study as Li Insertion Electrodes; Junjie Zhu, Zhonghua Lu, S. T. Aruna, Doron Aurbach, and Aharon Gedanken, Chem. Mater.**2000,** *12*, 2557-2566
23. Sonochemical Synthesis of SnO_2 Nanoparticles and Their Preliminary Study as Li Insertion Electrodes; Mukherjee, S.; Mukherjee, M. J. Phys.: Condens. Matter **2006***18* 11233–11242.
24. Surfactant-Assisted Synthesis of SnS Nanowires Grown on Tin Foils;Subhendu K. Panda, Anuja Datta, Apurba Dev, Soma Gorai, and Subhadra Chaudhuri, Crystal Growth & Design, Vol. 6, No. 9, 2006.
25. Synthesis and Characterization of -SnS Nanoparticles and Corresponding Thin Films; Jianquan Li, Henri Kessler, Microporous and Mesoporous Materials 27 (1999) 57–63.
26. Optical Properties of Solids; C. Tauc, North-Holland, Amsterdam (1972).
27. SnO_2 nanocrystals in SiO_2: A wide band gap quantum dot system; N. Chiodini, A. Paleari) D. Di Martino, and G. Spinolo, Appl. Phys. Lett., Vol. 81, No. 9, 26 August 2002.
28. Synthesis of a *ä*-SnS Polymorph by Electrodeposition; Jeffrey R. S. Brownson, CecileGeorges, and Claude Levy-Clement, Chem. Mater.**2006,** *18*, 6397-6402.